

# An examination of the chaotic magnetic field near the separatrix of magnetically confined plasmas

S.R.Hudson (PPPL) & Y. Suzuki (NIFS)

The most important theoretical/numerical calculation in the study of magnetically confined plasmas is to determine the magnetic field.

- 1) MHD equilibrium codes (such as HINT-2) determine the structure of the magnetic field, allowing for islands and chaotic fieldlines, in stellarators, perturbed tokamaks, . . .
- 2) It is always useful, and often essential, to know the chaotic structure of the fieldlines.
- 3) The efficiency, reliability and accuracy of such codes depend on accurate, robust, fast numerical routines.
  - 1) Constructing efficient subroutines requires tedious, careful work!

So, given the vector field,  $\mathbf{B}(\mathbf{x})$ , what are the properties of the integral-curves  $\equiv$  fieldlines?

1. The magnetic field,  $\mathbf{B}(\mathbf{x})$ , is a function of  $\mathbf{x} \equiv R \cos \phi \mathbf{i} + R \sin \phi \mathbf{j} + Z \mathbf{k}$ .

$$\mathbf{e}_R(\phi) \equiv \cos \phi \mathbf{i} + \sin \phi \mathbf{j}$$

2. Using cylindrical coordinates,  $\mathbf{e}_\phi(\phi) \equiv -\sin \phi \mathbf{i} + \cos \phi \mathbf{j}$   
 $\mathbf{e}_Z \equiv \mathbf{k}$

3. The magnetic field is specified by 3 functions,  $B^R$ ,  $B^\phi$  and  $B^Z$ :

$$\mathbf{B} \equiv B^R(R, \phi, Z) \mathbf{e}_R + B^\phi(R, \phi, Z) \mathbf{e}_\phi + B^Z(R, \phi, Z) \mathbf{e}_Z.$$

4. Really, only 2 functions are required; using  $\mathbf{B} = \nabla \times \mathbf{A}$  and gauge freedom

$$\text{e.g. } \mathbf{A} = \cancel{A_R \nabla R} + A_\phi \nabla \phi + A_Z \nabla Z + \cancel{\nabla g} = A_\phi \nabla \phi + A_Z \nabla Z. \quad (1)$$

[e.g. 2 functions  $\equiv$  toroidal, poloidal flux; Hamiltonian formalism,  $\mathbf{B} = \nabla \times (\psi \nabla \theta - \chi \times \nabla \zeta)$ ]

5. Given  $\mathbf{B}(\mathbf{x})$ , what are the properties of the fieldlines?

The vector field may be continuous & smooth, but the fieldlines may be chaotic!

Where is the magnetic axis? Are there “good-flux-surfaces”? Where is the plasma edge?

# The simplest diagnostic: Poincaré plot: from given $(R, Z)$ , follow along $\mathbf{B}$ a “distance” of $\Delta\phi=2\pi$

1. A magnetic fieldline,  $\mathbf{x}(\phi) = R(\phi)\mathbf{e}_R(\phi) + Z(\phi)\mathbf{e}_Z$ ,

is an integral curve of  $\mathbf{B}$ , i.e.  $\frac{d\mathbf{x}}{d\phi} = \mathbf{B}$ ,

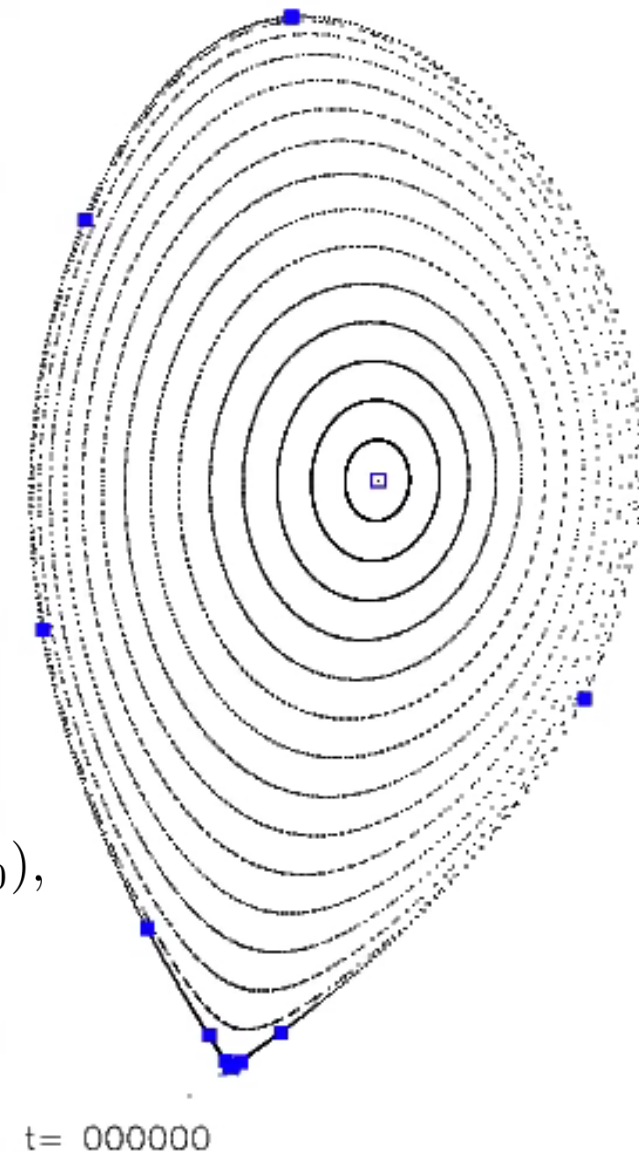
$$\dot{R} \equiv \frac{dR}{d\phi} \equiv \frac{B^R}{B^\phi}, \quad \dot{Z} \equiv \frac{dZ}{d\phi} \equiv \frac{B^Z}{B^\phi} \quad (1)$$

2. A Poincaré section is any plane  
“cutting across” the magnetic field.

For toroidal magnetic confinement devices,  
usually choose the plane  $\phi = 0$ .

3. From any starting point, e.g.  $(R, \phi, Z) = (R_0, 0, Z_0)$ ,  
integrate the o.d.e.s in Eqn(1), (e.g. Runge-Kutta)  
e.g. around  $N \approx 1000$ , toroidal periods,  $\Delta\phi = 2\pi$ .

Can “visualize” the magnetic field.



# The simplest diagnostic: Poincaré plot: from given $(R, Z)$ , follow along $\mathbf{B}$ a “distance” of $\Delta\phi=2\pi$

1. A magnetic fieldline,  $\mathbf{x}(\phi) = R(\phi)\mathbf{e}_R(\phi) + Z(\phi)\mathbf{e}_Z$ ,

is an integral curve of  $\mathbf{B}$ , i.e.  $\frac{d\mathbf{x}}{d\phi} = \mathbf{B}$ ,

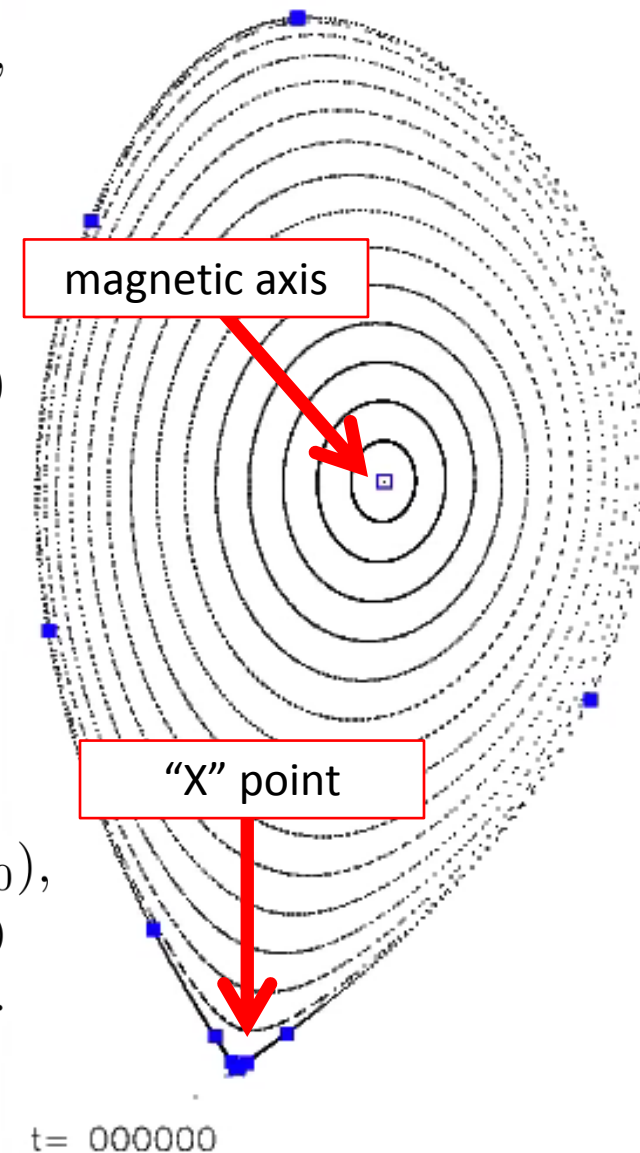
$$\dot{R} \equiv \frac{dR}{d\phi} \equiv \frac{B^R}{B^\phi}, \quad \dot{Z} \equiv \frac{dZ}{d\phi} \equiv \frac{B^Z}{B^\phi} \quad (1)$$

2. A Poincaré section is any plane “cutting across” the magnetic field.

For toroidal magnetic confinement devices,  
usually choose the plane  $\phi = 0$ .

3. From any starting point, e.g.  $(R, \phi, Z) = (R_0, 0, Z_0)$ ,  
integrate the o.d.e.s in Eqn(1), (e.g. Runge-Kutta)  
e.g. around  $N \approx 1000$ , toroidal periods,  $\Delta\phi = 2\pi$ .

Can “visualize” the magnetic field.



The magnetic axis and X-point are fixed points of the Poincaré mapping; which may be found, for example, using fieldline tracing + Newton iterations.

1. Introduce the mapping from  $\phi = 0$  to  $\phi = 2\pi$

$$\mathbf{M} : \begin{cases} R_1(R_0, Z_0) \equiv \int_0^{2\pi} \dot{R}(R, \phi, Z) d\phi, \text{ where } \dot{R} \equiv B^R / B^\phi \\ Z_1(R_0, Z_0) \equiv \int_0^{2\pi} \dot{Z}(R, \phi, Z) d\phi, \text{ where } \dot{Z} \equiv B^Z / B^\phi \end{cases} \quad (1)$$

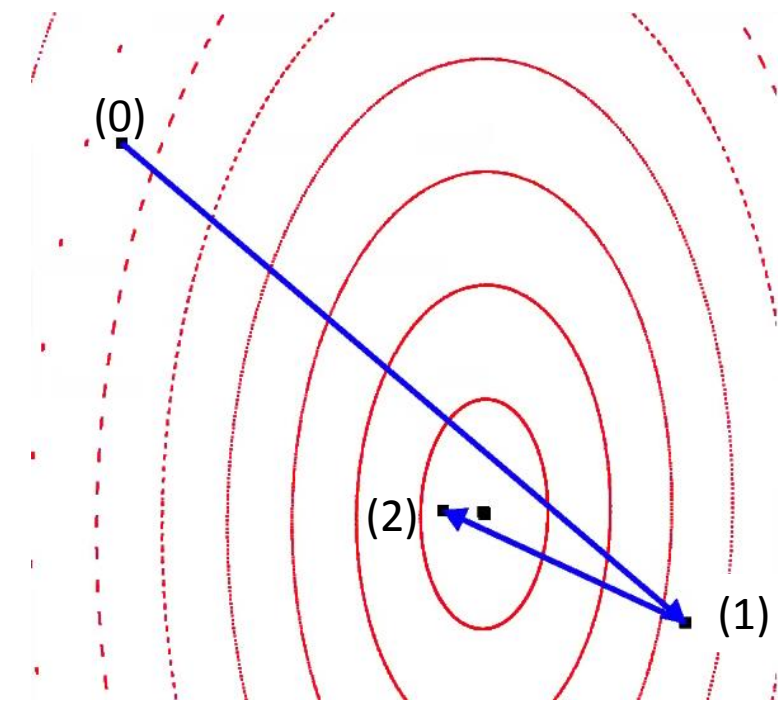
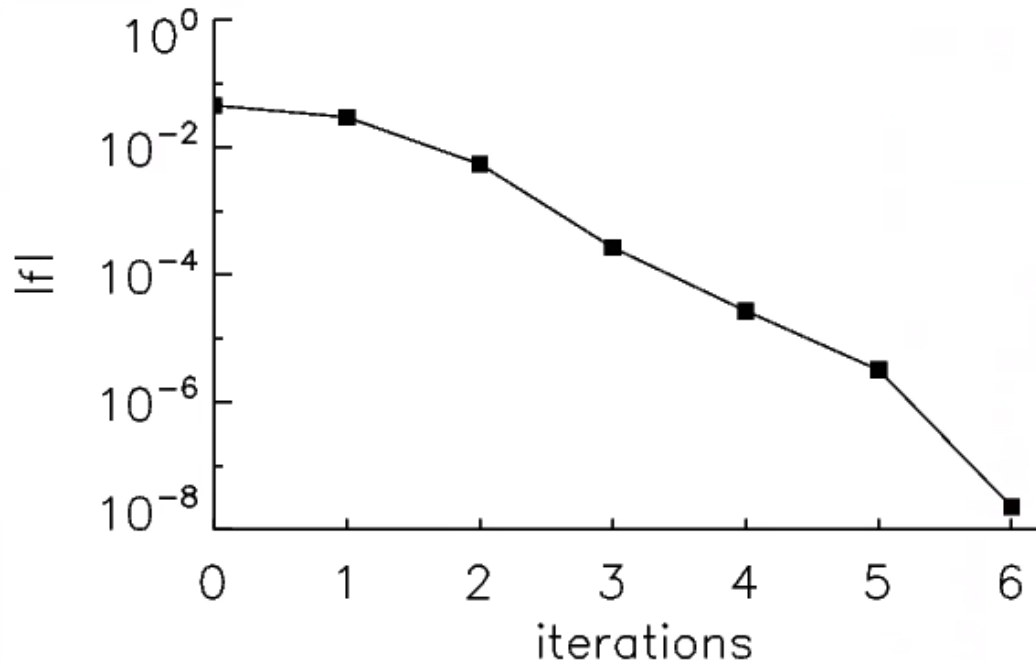
2. Magnetic fieldline starting at  $(R_0 + \delta R_0, Z_0 + \delta Z_0)$  closes on itself after  $\Delta\phi = 2\pi$  if

$$\begin{pmatrix} R_1 + \delta R_1 \\ Z_1 + \delta Z_1 \end{pmatrix} = \begin{pmatrix} R_1 \\ Z_1 \end{pmatrix} + \begin{pmatrix} \partial_{R_0} R_1, & \partial_{Z_0} R_1 \\ \partial_{R_0} Z_1, & \partial_{Z_0} Z_1 \end{pmatrix} \begin{pmatrix} \delta R_0 \\ \delta Z_0 \end{pmatrix} = \begin{pmatrix} R_0 + \delta R_0 \\ Z_0 + \delta Z_0 \end{pmatrix} \quad (2)$$

3. The behavior of fieldlines *nearby* a given fieldline is determined by the tangent mapping,  $\nabla \mathbf{M} \equiv \begin{pmatrix} \partial_{R_0} R_1, & \partial_{Z_0} R_1 \\ \partial_{R_0} Z_1, & \partial_{Z_0} Z_1 \end{pmatrix}$ ,

also determined by o.d.e. integration,  $d_\phi \nabla \mathbf{M} = \begin{pmatrix} \partial_R \dot{R} & \partial_Z \dot{R} \\ \partial_R \dot{Z} & \partial_Z \dot{Z} \end{pmatrix} \cdot \nabla \mathbf{M}$

# Example: locating the magnetic axis using fieldline tracing method + Newton iterations.



1. From suitable starting guess, iterations converge quickly.
2. To locate the magnetic axis using o.d.e. fieldline tracing method with Newton iterations requires  $\sim 10^3$  evaluations of  $\mathbf{B}(\mathbf{x})$ .

# “Global integration” is much faster:

the action integral is a functional of a curve in phase space.

1. The action,  $S$ , is line integral along a “trial” curve  $\{\mathcal{C} : q \equiv q(t)\}$ ,

$$\text{of the Lagrangian, } \mathcal{L} \equiv \underbrace{T(\dot{q}, q)}_{\text{kinetic}} - \underbrace{U(q, t)}_{\text{potential}}, \quad S \equiv \int_{\mathcal{C}} \mathcal{L}(q, \dot{q}, t) dt$$

2. For magnetic fields,  $\mathbf{B} = \nabla \times \mathbf{A}$ ,  $S \equiv \int_{\mathcal{C}} \mathbf{A} \cdot \frac{d\mathbf{x}}{d\phi} d\phi$ , along  $\{\mathcal{C} : R \equiv \mathbf{R}(\phi), Z \equiv \mathbf{Z}(\phi)\}$

3. Action extremizing curves  $\equiv$  magnetic fieldlines.

4. Use a global representation, e.g.  $R(\phi) \equiv \sum \mathbf{R}_n \cos(n\phi)$  and  $Z(\phi) \equiv \sum \mathbf{Z}_n \sin(n\phi)$ ,

$$\frac{\partial S}{\partial \mathbf{R}_n} = \int_0^{2\pi} (B^Z - B^\phi \dot{Z}) R \cos(n\phi) d\phi, \quad \frac{\partial S}{\partial \mathbf{Z}_n} = \int_0^{2\pi} (-B^R + B^\phi \dot{R}) R \sin(n\phi) d\phi \quad (1)$$

5. Can use multi-dimensional Newton method, and FFT's, to set

$$F_{\mathbf{R}, n} \equiv [(B^Z - B^\phi \dot{Z}) R]_n = 0$$

$$F_{\mathbf{Z}, n} \equiv [(-B^R + B^\phi \dot{R}) R]_n = 0$$

6. About  $100\times$  faster: requires  $\sim 10^1$  evaluations of  $\mathbf{B}(\mathbf{x})$

→ Vector potential,  $\mathbf{A}$ , is not required;

→ global integration comparatively immune to exponential errors.

The tangent mapping determines the behavior of nearby fieldlines.

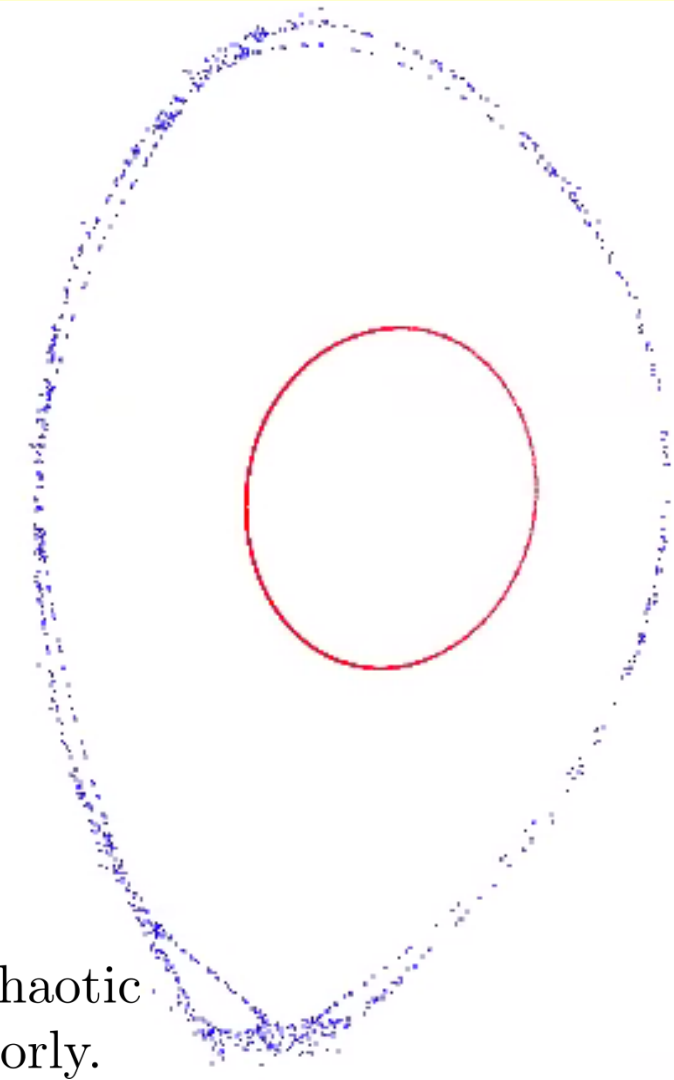
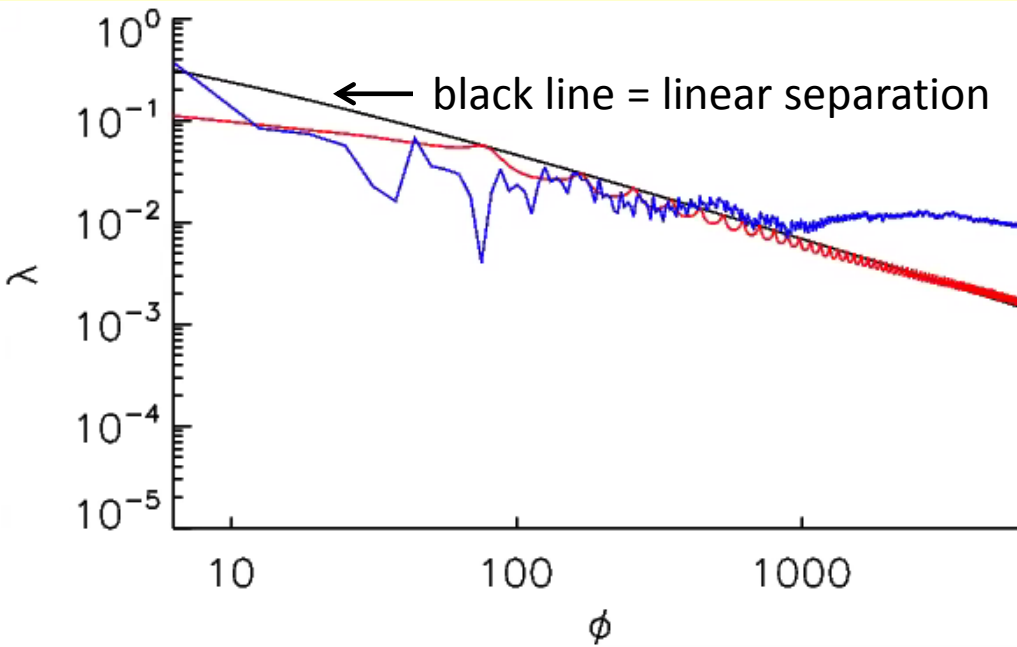
Chaos: nearby fieldlines diverge exponentially.

1. The Lyapunov exponent,  $\lambda$ , determines the average rate of exponential separation of initially-nearby fieldlines, e.g.  $\mathbf{x}(0)$  and  $\mathbf{x}(0) + \delta\mathbf{x}(0)$ ,

Assuming  $\underbrace{|\delta\mathbf{x}(\phi)| \approx e^{\lambda\phi} |\delta\mathbf{x}(0)|}_{\text{exponential}}$ , then  $\lambda \equiv \lim_{\phi \rightarrow \infty} \lim_{\delta x(0) \rightarrow 0} \frac{1}{\phi} \log \frac{\delta x(\phi)}{\delta x(0)}$  (1)

2. Rather than following nearby fieldlines and then taking  $\lim_{\delta x(0) \rightarrow 0}$   
it is better to work in “tangent space”,  $\delta x(\phi) \equiv \nabla \mathbf{M}(\phi) \cdot \delta x(0)$ . (2)
3. If  $\lambda > 0$ , there is extreme sensitivity to initial conditions.
4. For some fieldlines (e.g. on good-flux-surfaces) nearby fieldlines diverge *linearly*,  
e.g.  $\delta x(\phi) \approx \text{const. } \phi$ . Eqn(1) gives  $\lambda(\phi) \approx \log \phi/\phi$ .

The Lyapunov exponent can distinguish chaotic trajectories,  
but it is computationally costly.



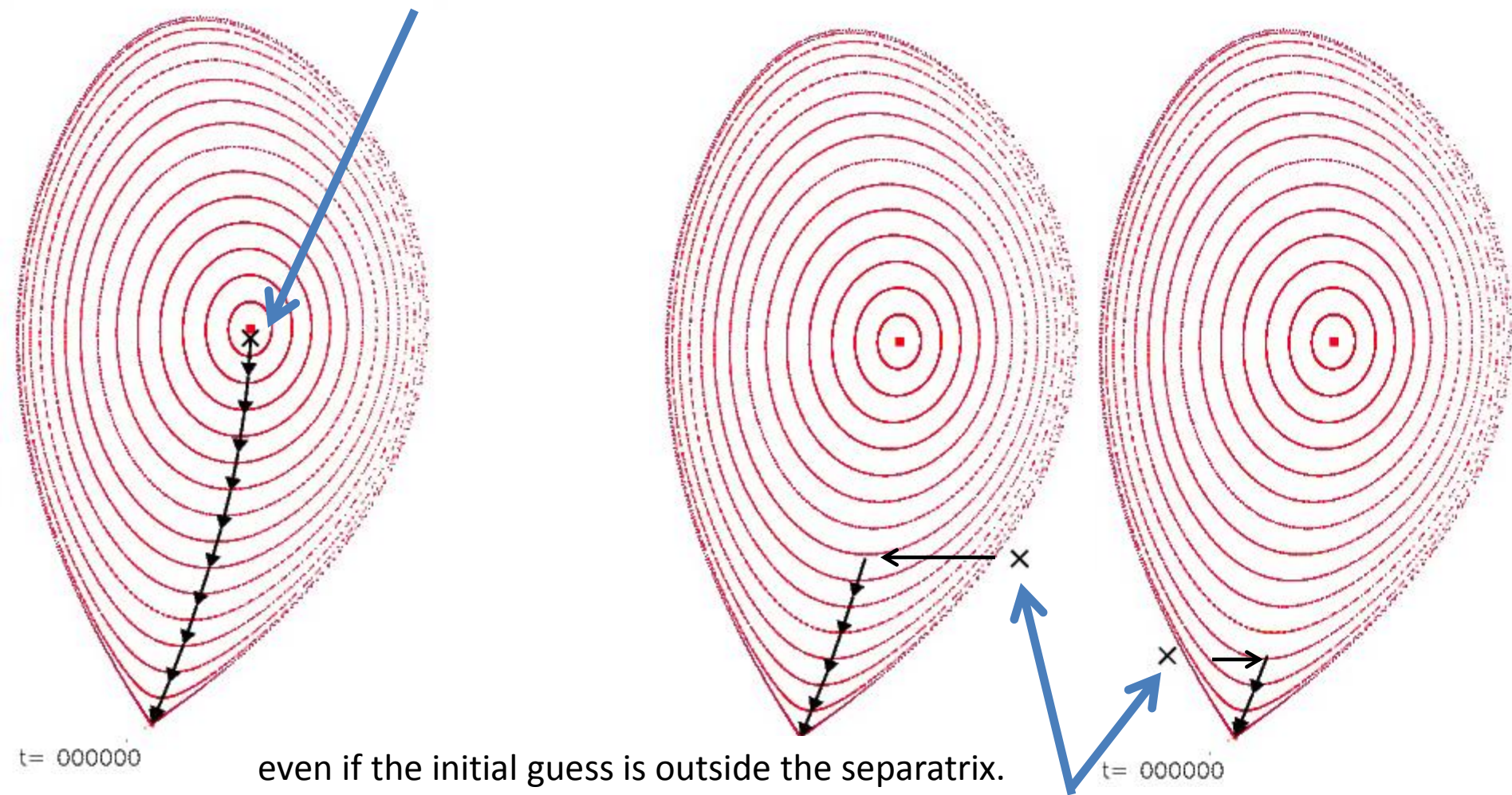
1. A large distance in  $\phi$  is required to distinguish “linear” motion from weakly-“exponential”.
2. Fieldline tracing methods  
(e.g. Poincaré plots, Lyapunov exponents, . . .)  
are widely used to determine the structure of chaotic fields, but they are very costly and perform poorly.

# “Global integration” can robustly find the action minimizing curve = X-point

1. Action integral:  $S[\mathbf{R}_n, \mathbf{Z}_n] \equiv \int_0^{2\pi} \mathbf{A} \cdot \frac{d\mathbf{x}}{d\phi} d\phi.$
2.  $\frac{dS}{d\mathbf{R}_n} \equiv \underbrace{\int_0^{2\pi} (+B^Z - B^\phi \dot{Z}) \cos(n\phi)}_{F_{R,n}}, \quad \frac{dS}{d\mathbf{Z}_n} \equiv \underbrace{\int_0^{2\pi} (-B^R + B^\phi \dot{R}) \sin(n\phi)}_{F_{Z,n}}$
3. Gradient flow:  $\frac{d\mathbf{R}_n}{d\tau} \equiv -F_{R,n}[\mathbf{R}_n, \mathbf{Z}_n], \quad \frac{d\mathbf{Z}_n}{d\tau} \equiv -F_{Z,n}[\mathbf{R}_n, \mathbf{Z}_n] : \quad \frac{dS[\mathbf{R}_n, \mathbf{Z}_n]}{d\tau} < 0.$
4. However, for the action to have a minimum, the curve must be constrained:  
 must choose  $R(\phi) \equiv \mathbf{R}[\mathbf{Z}(\phi)]$ , e.g.  $F_R[\mathbf{R}[\mathbf{Z}(\phi)], \mathbf{Z}(\phi)] = 0,$   
 or  $Z(\phi) \equiv \mathbf{Z}[\mathbf{R}(\phi)]$ , e.g.  $F_Z[\mathbf{R}(\phi), \mathbf{Z}[\mathbf{R}(\phi)]] = 0.$  } These constraints must be invertible.
5. Even (i) from a “poor” initial guess, and (ii) with  $\nabla \cdot \mathbf{B} \approx \epsilon$ , and (iii) with “strong chaos”, i.e. large- $\lambda$ ; this method will robustly find the action-minimizing, X-curve.  
 (This will be useful for locating the homoclinic tangle, but the “gradient-flow” method is slow.)

# “Global integration” can robustly find the action minimizing curve = X-point

From “arbitrary” initial guess,  
e.g. from close to the O-point,  
the gradient-flow method converges on X-point,



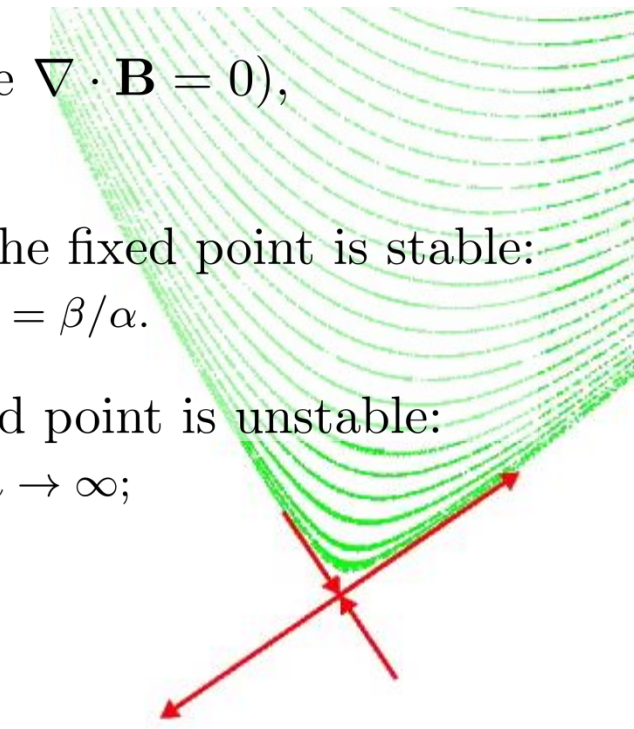
The magnetic axis is a “stable” fixed point (usually), and the X-point is “unstable”.

Consider the eigenvalues of tangent mapping:

1. Consider following a fieldline nearby a fixed point,  $\mathbf{x}_0 + \delta\mathbf{x}$ , around many toroidal periods:

$$\underbrace{\nabla\mathbf{M} \cdot \dots \cdot \nabla\mathbf{M}}_{\text{tangent mapping}} \cdot \delta\mathbf{x} = (\nabla\mathbf{M})^n \cdot \delta\mathbf{x} = (\nabla\mathbf{M})^n \cdot \underbrace{(a \mathbf{v}_u + b \mathbf{v}_s)}_{\text{eigenvectors}} = a \lambda_u^n \mathbf{v}_u + b \lambda_s^n \mathbf{v}_s$$

2. The determinant,  $|\nabla\mathbf{M}| = 1$  at fixed points (because  $\nabla \cdot \mathbf{B} = 0$ ), so the eigenvalues are either:
  - i. complex conjugates,  $\lambda = \alpha + \beta i$ ,  $\lambda = \alpha - \beta i$ , and the fixed point is stable: nearby trajectories rotate: rotational-transform on axis,  $\tan \tau = \beta/\alpha$ .
  - ii. real reciprocals,  $\lambda_u > 1$  and  $\lambda_s = 1/\lambda_u$ , and the fixed point is unstable: nearby trajectories diverge:  $\lambda_u^n \rightarrow \infty$  as  $n \rightarrow \infty$ ,  $\lambda_s^n \rightarrow 0$  as  $n \rightarrow \infty$ ;  $\mathbf{v}_u$  indicates unstable direction,  $\mathbf{v}_s$  indicates stable direction.



The **stable/unstable** direction forwards in  $\phi$  is the **unstable/stable** direction backwards in  $\phi$ .

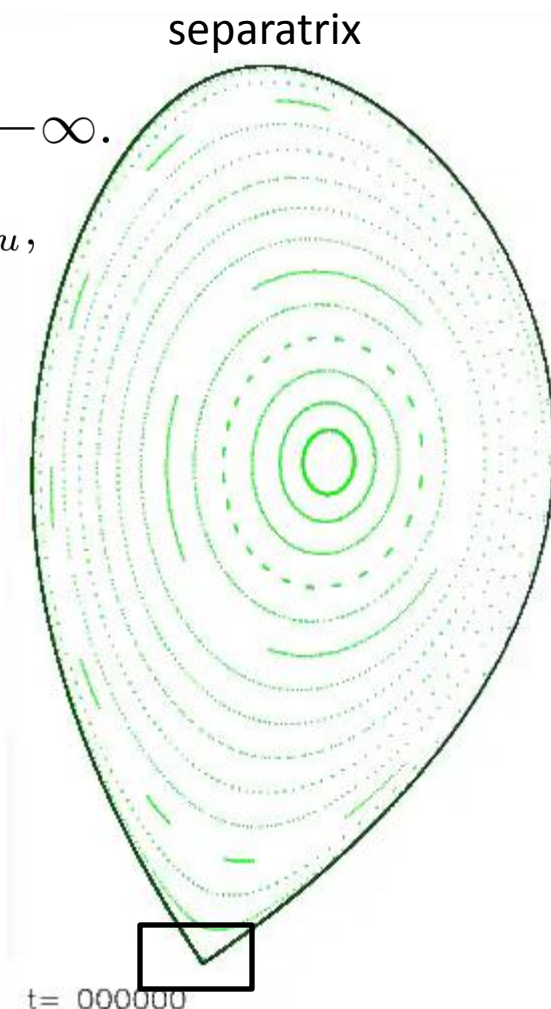
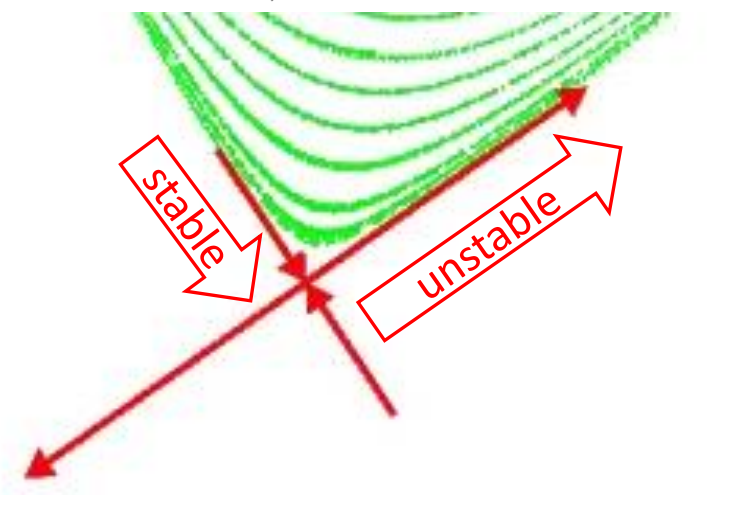
1.  $\mathbf{x} \in$  “stable manifold” if  $\mathbf{M}^n(\mathbf{x}) \rightarrow \mathbf{x}_0$  as  $n \rightarrow +\infty$ .

all magnetic fieldlines with “starting point”  $\mathbf{x} = \mathbf{x}_0 + d \mathbf{v}_s$ ,  
where  $d \in [\epsilon \lambda_s, \epsilon]$ , and follow *backwards* in  $\phi$ .

2.  $\mathbf{x} \in$  “unstable manifold” if  $\mathbf{M}^n(\mathbf{x}) \rightarrow \mathbf{x}_0$  as  $n \rightarrow -\infty$ .

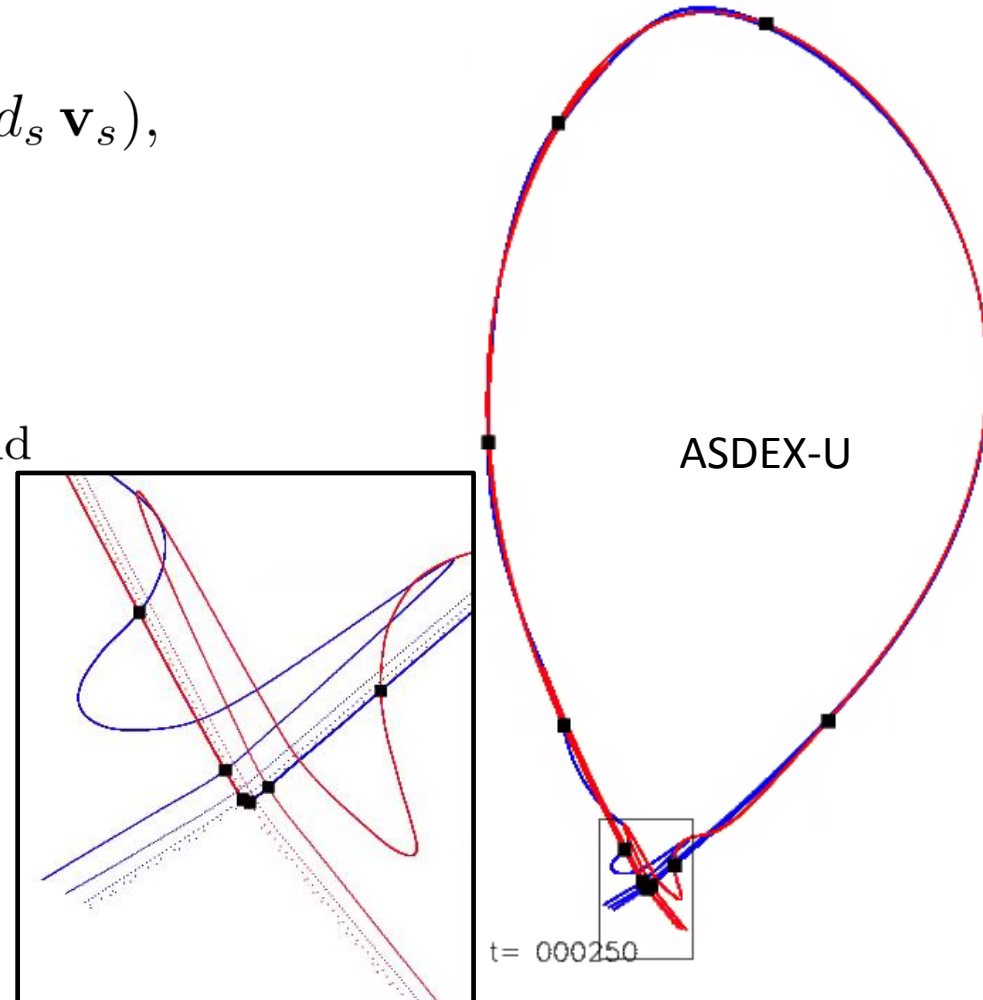
all magnetic fieldlines with “starting point”  $\mathbf{x} = \mathbf{x}_0 + d \mathbf{v}_u$ ,  
where  $d \in [\epsilon/\lambda_u, \epsilon]$ , and follow *forwards* in  $\phi$ .

3. For the integrable case, the unstable manifold leads into the stable manifold, and there is a “clean” separatrix.

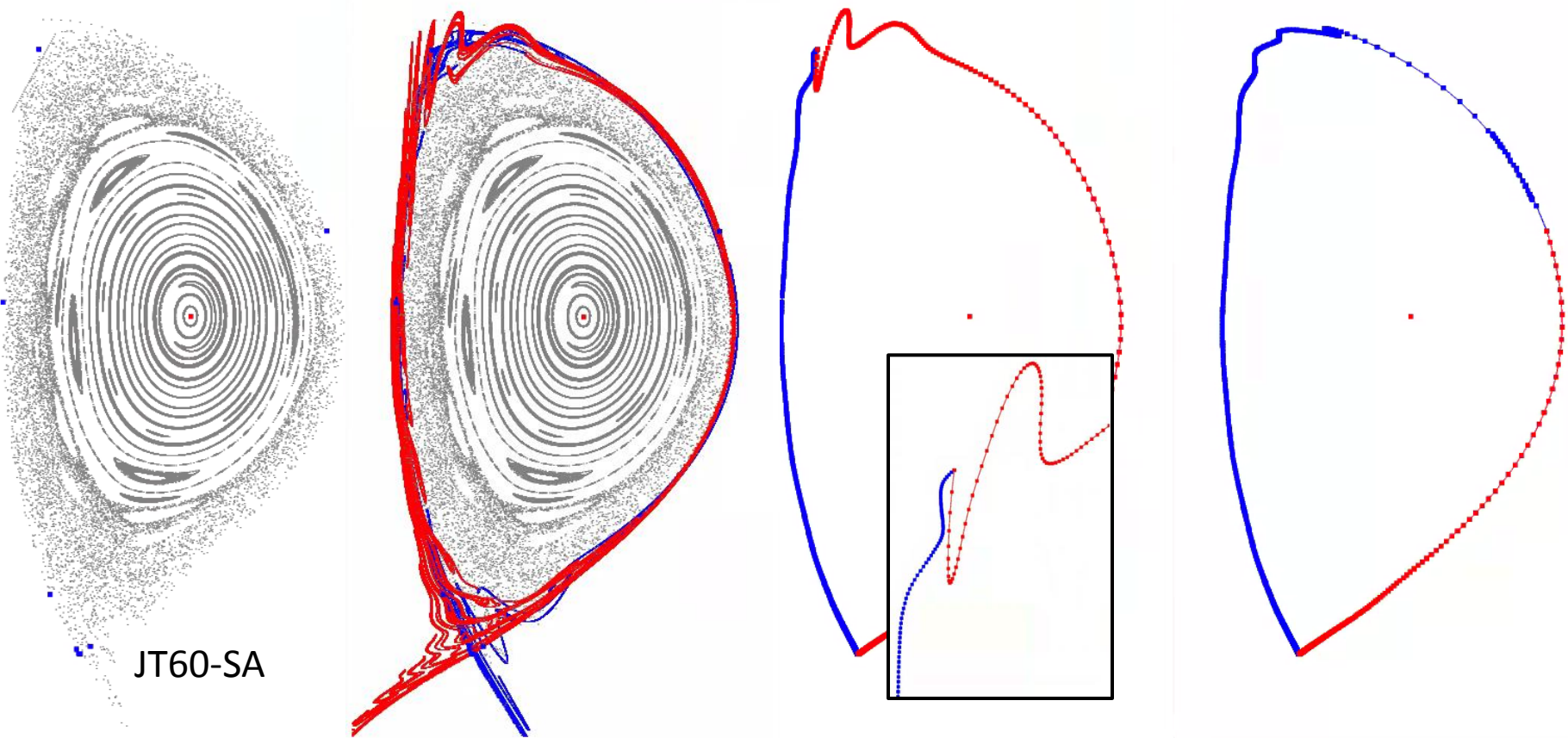


For perturbed magnetic fields, the separatrix splits.  
A “partial” separatrix can be constructed.

1. “Homoclinic” points,  $\mathbf{x}_h \equiv$  intersection of stable, unstable manifolds,  
 $\mathbf{M}^n(\mathbf{x}_h) \rightarrow \mathbf{x}_0$  as  $n \rightarrow \pm\infty$ .
2. To locate  $\mathbf{x}_h$ , find  $(d_u, d_s)$ ,  
 $\mathbf{M}^{+i}(\mathbf{x}_0 + d_u \mathbf{v}_u) = \mathbf{M}^{-j}(\mathbf{x}_0 + d_s \mathbf{v}_s)$ ,  
if  $\mathbf{x}_h$  is homoclinic,  
so is  $\mathbf{M}^k(\mathbf{x}_h), \forall k$ .
3. Partial separatrix  
= “smooth” part of unstable manifold  
+ “smooth” part of stable manifold.



For JT60-SA, the partial separatrix is strongly influenced by an “almost” double-null.



# Consider heat transport: rapid transport along the magnetic field, slow transport across the magnetic field.

1. Transport along the magnetic field is unrestricted:  
e.g. parallel random walk with long steps  $\approx$  collisional mean free path.
2. Transport across the magnetic field is very small:  
e.g. perpendicular random walk with short steps  $\approx$  Larmor radius.

3. Simplest transport model: anisotropic diffusion,

$$\boxed{\frac{\partial T}{\partial t} = \nabla \cdot (\kappa_{\parallel} \nabla_{\parallel} T + \kappa_{\perp} \nabla_{\perp} T) + S}, \quad \kappa_{\perp}/\kappa_{\parallel} \sim 10^{-10}, \quad T \equiv \text{temperature}; \quad S \equiv \text{source};$$

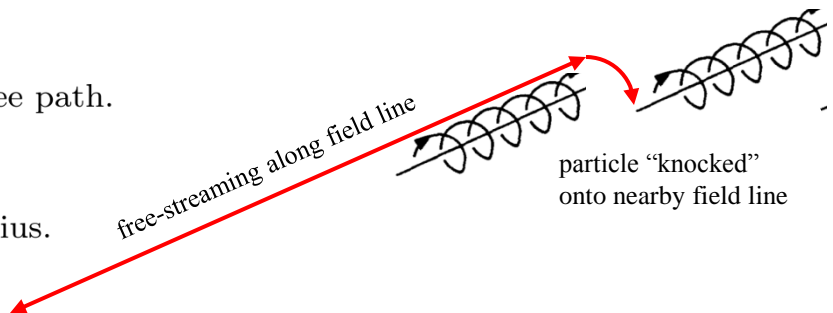
4. Because of the extreme anisotropy, even the *simplest* model of transport presents numerical challenge!  
 $\rightarrow$  extreme numerical resolution is required.
5. For computational efficiency, introduce “local fieldline coordinates”.

Construct coordinates  $(\alpha, \beta, \zeta)$  s.t.  $\mathbf{B} \equiv \nabla\alpha \times \nabla\beta$ , by local fieldline tracing;

Parallel and perpendicular directions are treated separately,  $\mathbf{B} \cdot \nabla \equiv B^{\phi} \partial_{\zeta}$ , which reduces numerical diffusion.

The parallel diffusion operator becomes  $\nabla_{\parallel}^2 T = B^{\phi} \frac{\partial}{\partial \zeta} \left( \frac{B^{\phi}}{B^2} \frac{\partial T}{\partial \zeta} \right)$ .

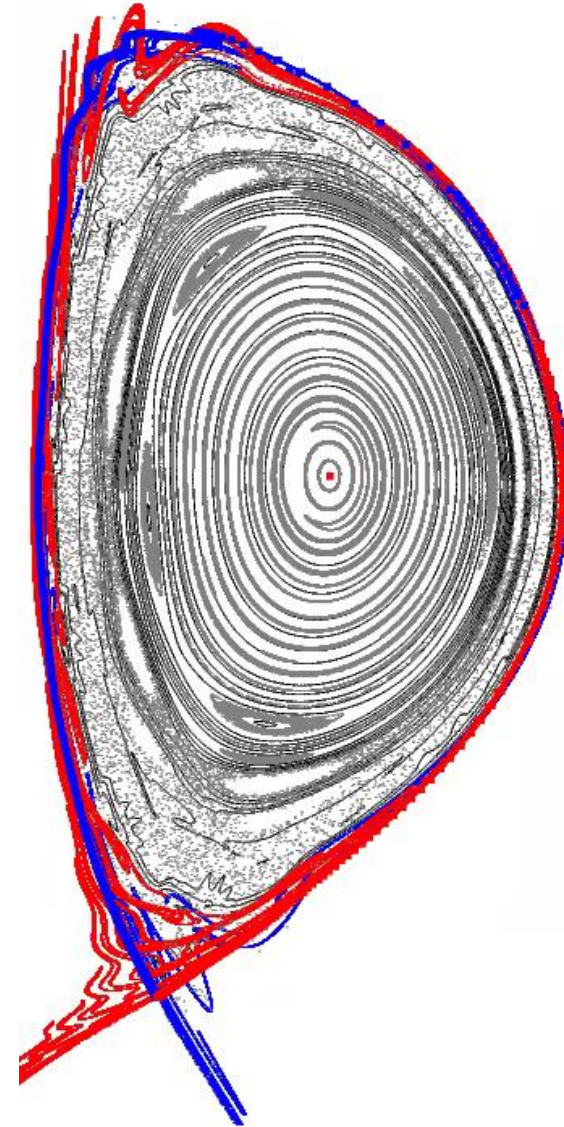
(This numerical algorithm is currently being benchmarked for speed & accuracy with existing HINT algorithm.)



# Anisotropic heat transport + unstable manifold = ?

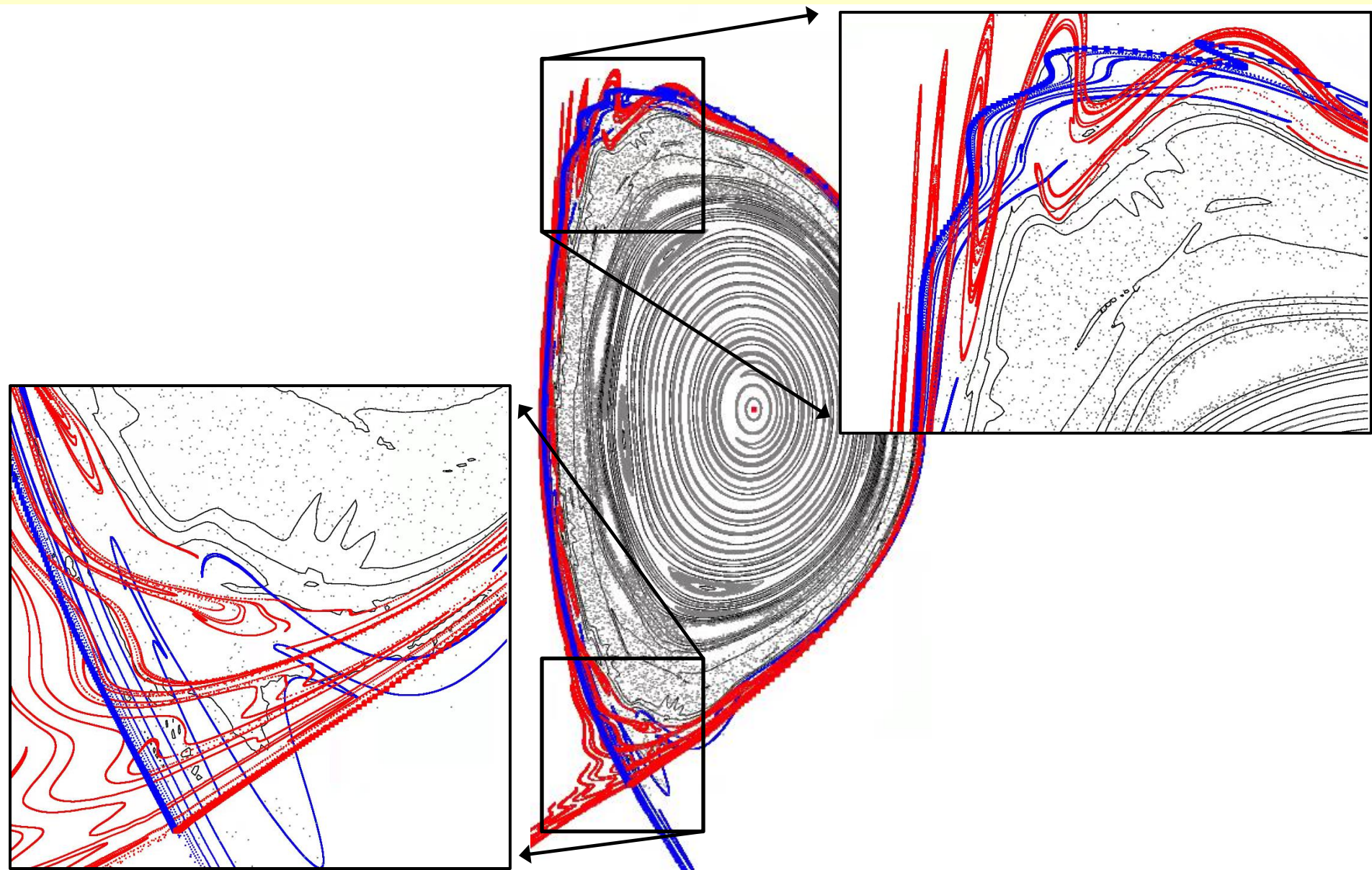
## What is the temperature in the “chaotic edge” ?

1. JT60-SA with chaotic edge,  $\mathbf{B}$  calculated using HINT-2.
2. To investigate the effect of the unstable manifold on  $T$ 
  - (a) must numerically calculate heat transport ✓
  - (b) must accurately construct unstable manifold ✓
3. These tasks are completed and implemented into HINT-2.
  - now we can make quantitative calculations
  - ongoing research.



Anisotropic heat transport + unstable manifold = ?

What is the temperature in the “chaotic edge” ?



# OCULUS: the eye into chaos

1. OCULUS<sup>©</sup> : a user-friendly, *theoretically-sophisticated*, imaginatively-named, library of subroutines for analyzing the structure of non-integrable (chaotic) magnetic fields
  - \* freely available online at <http://w3.pppl.gov/~shudson/Oculus/oculus.pdf>
  - \* 9 subroutines are presently available
2. This library is integrated into HINT-2, M3D-C<sub>1</sub>, SPEC, and NIMROD (under construction), . . .
3. Our long-term goal is for all high-performance codes to use shared, co-developed, freely-available, numerical libraries.
4. A community-based approach to large-scale computing.
  1. Many codes ask the same questions, i.e. need the same subroutines.

Where is the last, closed, flux surface? Where is the unstable manifold? Where are the magnetic islands, and how big are they? Where is the magnetic axis? How “chaotic” is the magnetic field?

# Oculus: The Eye into Chaos

S.R. Hudson\*

*Princeton Plasma Physics Laboratory, PO Box 451, Princeton NJ 08543, USA*

Y. Suzuki†

*National Institute for Natural Sciences, National Institute for Fusion Sciences, 322-6 Oroshi, Toki, 509-5292, Japan*

(Dated: August 26, 2015)

The **Oculus** package is a suite of magnetic field diagnostic subroutines (under continual development) for non-integrable, toroidal magnetic fields used in the numerical simulation of magnetic confinement of fusion-research plasmas. **Oculus** is freely distributed, with the expectation that users will promptly inform the developer(s) of any errors.

Suggestions and requests are welcome, indeed encouraged!

## Contents

<b>I. user supplied magnetic field</b>	1
<b>II. macro expansion and compilation</b>	2
<b>III. error flag</b>	2
<b>IV. subroutines</b>	2
A. ga00aa : find the magnetic axis;	2
B. ho00aa : find the homoclinic points (of the stable/unstable manifold);	6
C. ec00aa : find action extremizing curves using global integration;	9
D. tr00aa : measure rotational-transform;	11
E. pp00aa : fieldline tracing for Poincaré plot, calculate Lyapunov exponent;	13
F. qf00aa : construct quadratic-flux minimizing surface using pseudo fieldline following algorithm;	15
G. aa00aa : construct vector potential in toroidal coordinates;	16
H. ad00aa : anisotropic diffusion using locally-field-aligned coordinates;	17
I. bc00aa : interpolate set of toroidal surfaces;	21
<b>References</b>	22

So far, have used cylindrical coordinates  $(R, \phi, Z)$ .  
Is it better to use toroidal coordinates,  $(\psi, \theta, \phi)$  ?

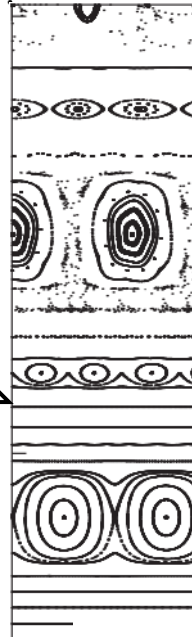
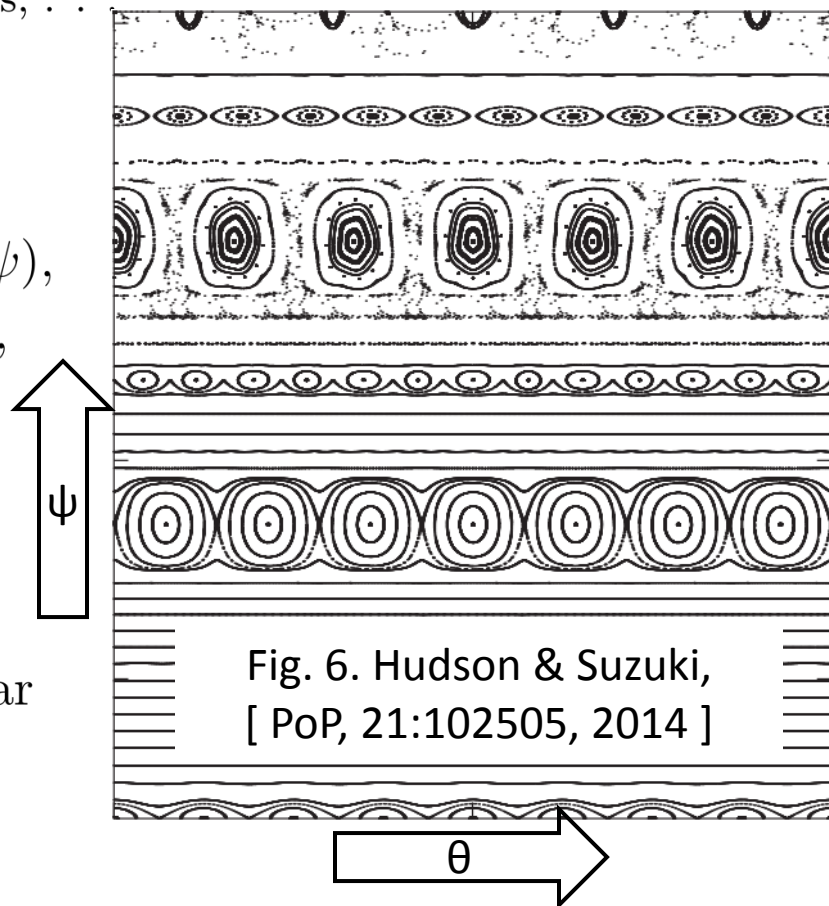
1. Toroidal coordinates (flux-coordinates) can be very useful,  
e.g. straight-fieldline coordinates, Boozer coordinates, . . .
    - i. easy to locate periodic orbits, cantori,
    - ii. easy to compute island widths,
    - iii. to a good approximation, pressure=  $p(\psi)$ ,
  2. Previously constructed “chaotic coordinates”  
 $\equiv$  “almost” straight-fieldline coordinates  
for the chaotic edge of LHD.
  3. But, straight-fieldline coordinates are singular  
at the separatrix!

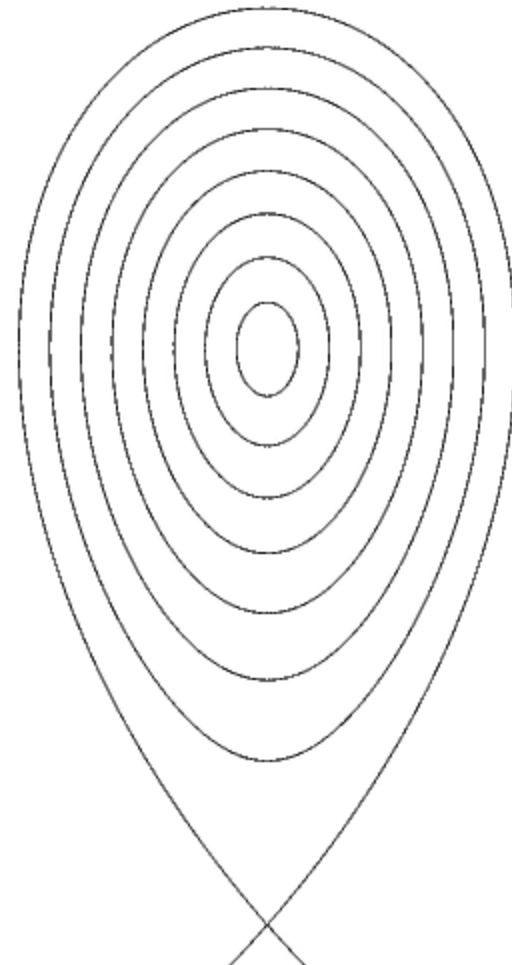
Fig. [PC]



This time, my research goal is to treat the coordinate singularity at the separatrix .

Question: can a toy Hamiltonian be “fit” to the partial separatrix to provide suitable, “background” toroidal coordinates?

“Toy”

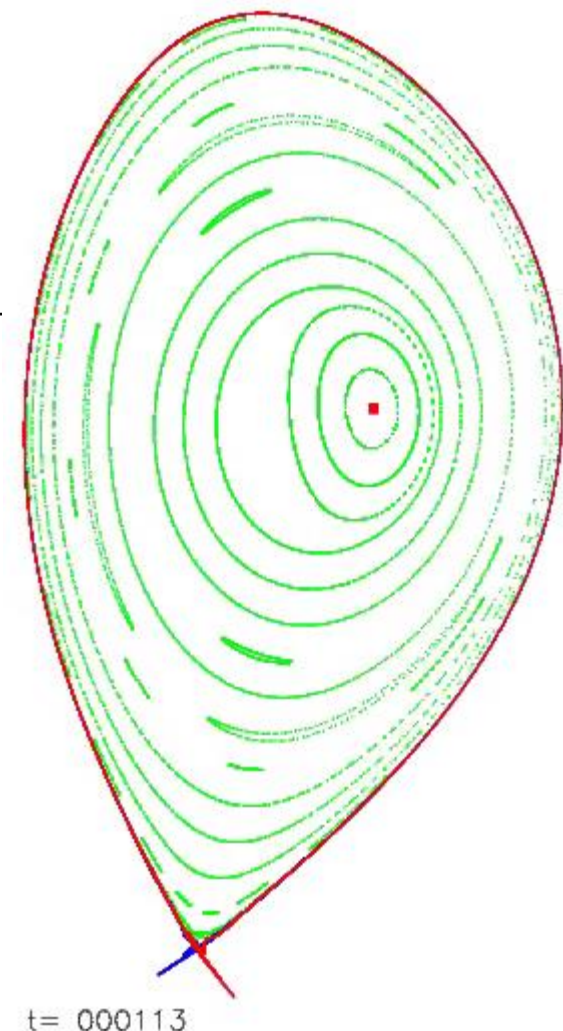


1. Consider “toy” Hamiltonian:

$$H_T \equiv \frac{1}{2}x^2 + 2y^3 + 3y^2. \quad (1)$$

Action-angle coordinates for  $H_T$  have same singular structure as straight-fieldline coordinates for single-null tokamaks.

ASDEX-U



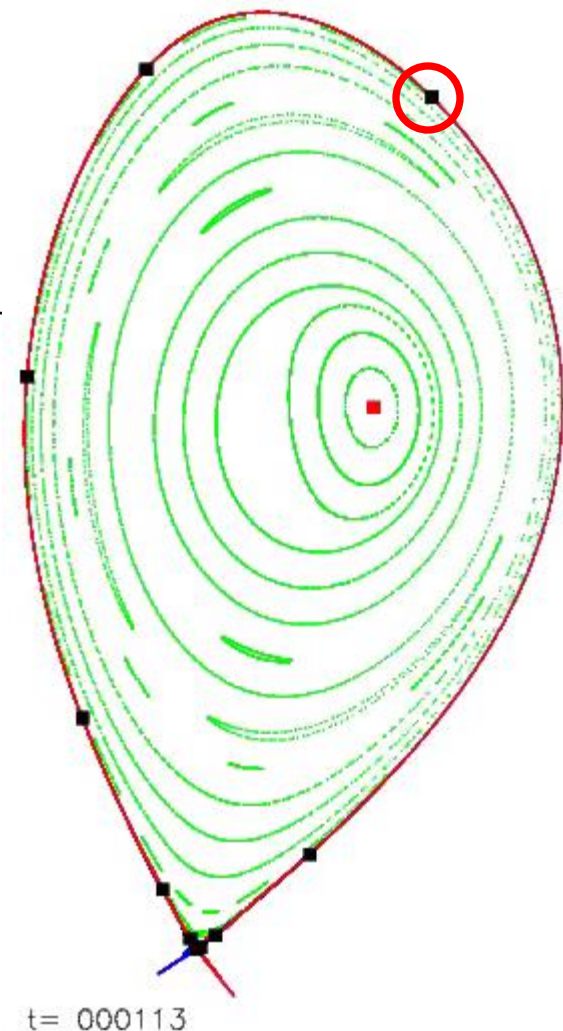
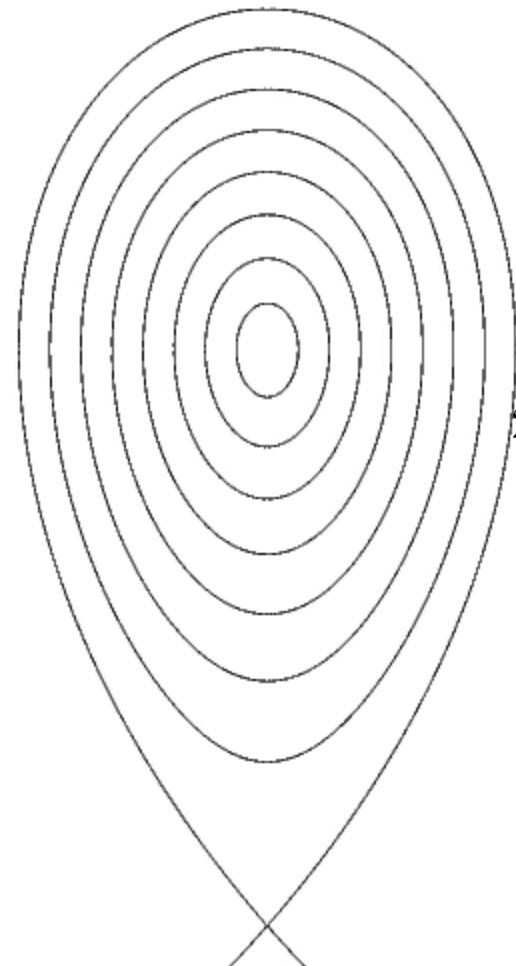
# Question: can a toy Hamiltonian be “fit” to the partial separatrix to provide suitable, “background” toroidal coordinates?

1. Consider “toy” Hamiltonian:

$$H_T \equiv \frac{1}{2}x^2 + 2y^3 + 3y^2. \quad (1)$$

Action-angle coordinates for  $H_T$  have same singular structure as straight-fieldline coordinates for single-null tokamaks.

2. Construct points that lie on stable, unstable manifold up to “primary intersection point”



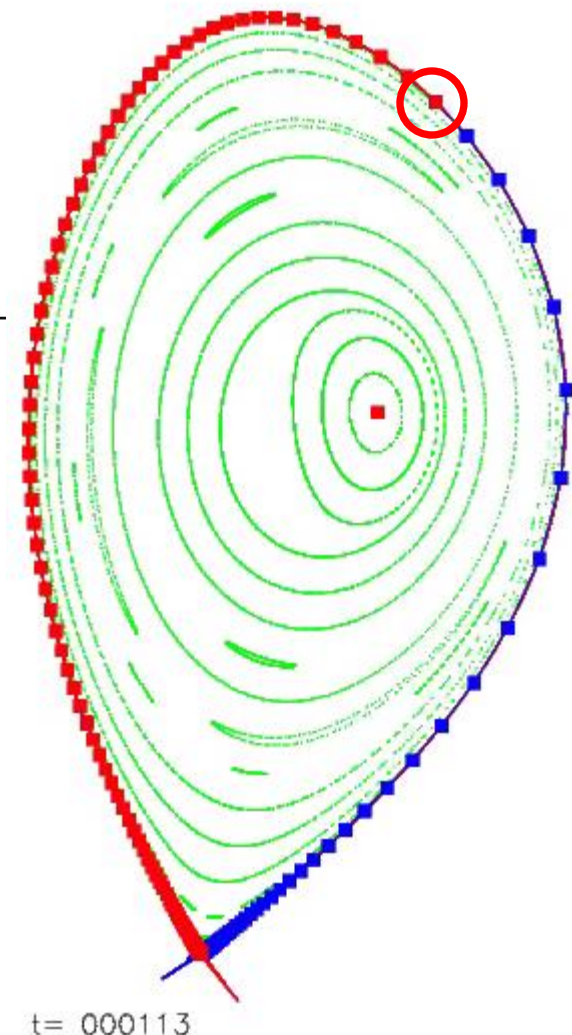
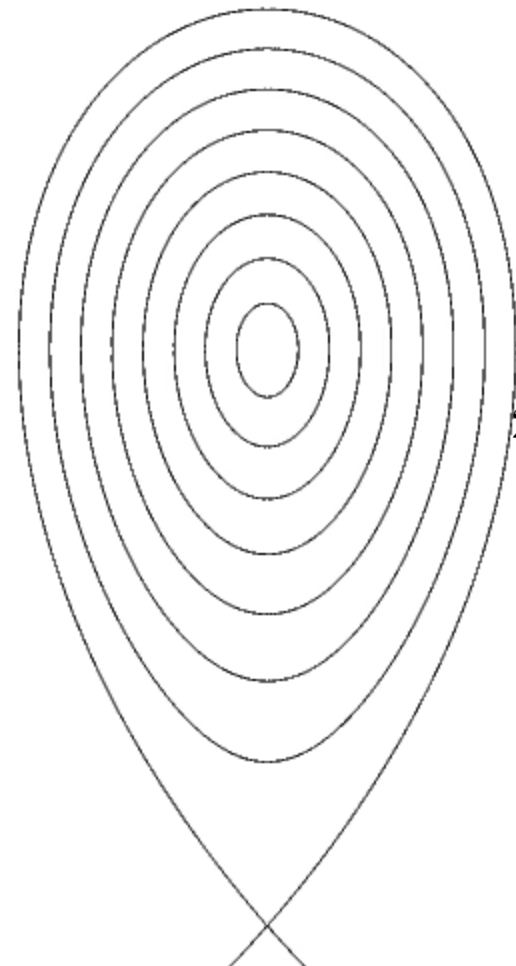
# Question: can a toy Hamiltonian be “fit” to the partial separatrix to provide suitable, “background” toroidal coordinates?

1. Consider “toy” Hamiltonian:

$$H_T \equiv \frac{1}{2}x^2 + 2y^3 + 3y^2. \quad (1)$$

Action-angle coordinates for  $H_T$  have same singular structure as straight-fieldline coordinates for single-null tokamaks.

2. Construct points that lie on stable, unstable manifold up to “primary intersection point”



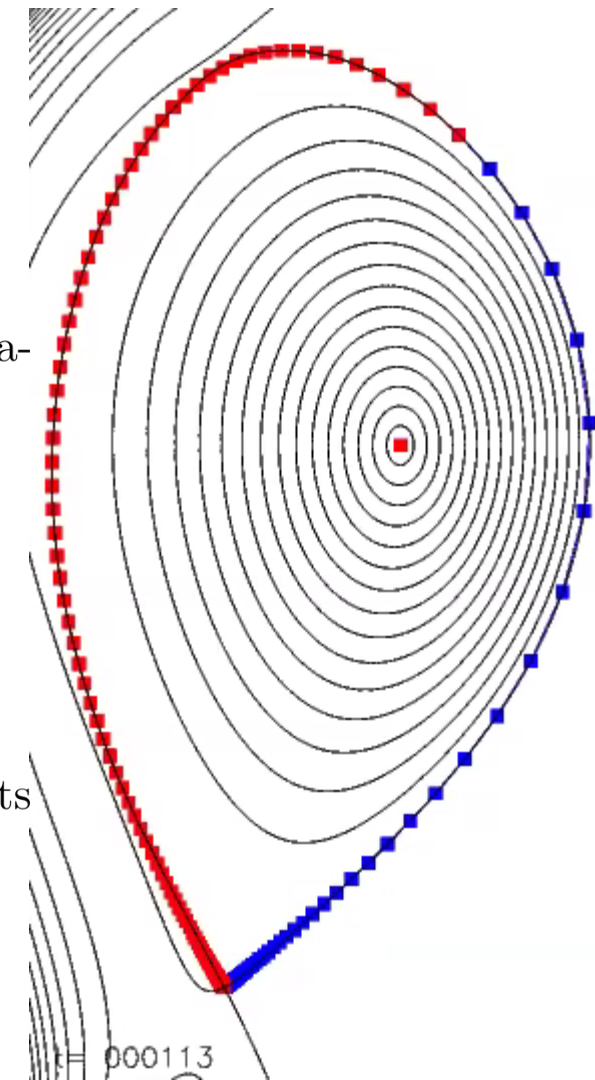
# Question: can a toy Hamiltonian be “fit” to the partial separatrix to provide suitable, “background” toroidal coordinates?

1. Consider “toy” Hamiltonian:

$$H_T \equiv \frac{1}{2}x^2 + 2y^3 + 3y^2. \quad (1)$$

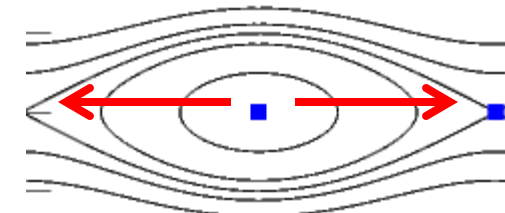
Action-angle coordinates for  $H_T$  have same singular structure as straight-fieldline coordinates for single-null tokamaks.

2. Construct points that lie on stable, unstable manifold up to “primary intersection point”
3. Fit “Hamiltonian”,  $H = \sum_{i,j} h_{i,j} x^i y^j$ , to “partial” separatrix, with constraints at  $X$ -point and  $O$ -points.
4. Contours of  $H$  provide suitable “background”, toroidal coordinates for further calculations.



Ghost surfaces, a class of almost-invariant surface, are defined by an action-gradient flow between the action minimax and minimizing fieldline.

1. Action,  $S[\mathcal{C}] \equiv \int_{\mathcal{C}} \mathbf{A} \cdot d\mathbf{l}$ , and action gradient,  $\frac{\partial S}{\partial \theta} \equiv \sqrt{g}B^\rho - \dot{\rho}B^\zeta$ .
2. Enforce  $\frac{\partial S}{\partial \rho} \equiv \dot{\theta}B^\zeta - \sqrt{g}B^\theta = 0$ , i.e. invert  $\dot{\theta} \equiv B^\theta/B^\zeta$  to obtain  $\rho = \rho(\dot{\theta}, \theta, \zeta)$ ; so that trial curve is completely described by  $\theta(\zeta)$ , and the action reduces from  $S \equiv S[\rho(\zeta), \theta(\zeta)]$  to  $S \equiv S[\theta(\zeta)]$
3. Define action-gradient flow: 
$$\boxed{\frac{\partial \theta(\zeta; \tau)}{\partial \tau} \equiv -\frac{\partial S[\theta]}{\partial \theta}},$$
 where  $\tau$  is an arbitrary integration parameter.
4. Ghost-surfaces are constructed as follows:
  - i. Begin at action-minimax (“O”, “not-always-stable”) periodic fieldline, which is a saddle;
  - ii. initialize integration in decreasing direction (given by negative eigenvalue/vector of Hessian);
  - iii. the entire curve “flows” down the action gradient,  $\partial_\tau \theta = -\partial_\theta S$ ;
  - iv. action is decreasing,  $\partial_\tau S < 0$ ;
  - v. finish at action-minimizing (“X”, unstable) periodic fieldline.
  - vi. ghost surface described by  $\mathbf{x}(\zeta, \tau)$ , where  $\tau$  is a fieldline label.



# The construction of extremizing curves of the action generalized extremizing surfaces of the quadratic-flux

1.  $\delta S = \int_C d\zeta \left( \delta\theta \frac{\partial S}{\partial\theta} + \delta\rho \frac{\partial S}{\partial\rho} \right)$ , where  $\boxed{\frac{\partial S}{\partial\theta} \equiv \sqrt{g}B^\rho - \dot{\rho}\sqrt{g}B^\zeta}$  and  $\boxed{\frac{\partial S}{\partial\rho} \equiv \dot{\theta}\sqrt{g}B^\zeta - \sqrt{g}B^\theta}$ .
2. Extremal curves satisfy  $\frac{\partial S}{\partial\theta} = 0$ , i.e.  $\dot{\rho} = B^\rho/B^\zeta$ , and  $\frac{\partial S}{\partial\rho} = 0$ , i.e.  $\dot{\theta} = B^\theta/B^\zeta$ .
3. Introduce toroidal surface,  $\rho \equiv P(\theta, \zeta)$ , and *family* of angle curves,  $\theta_\alpha(\zeta) \equiv \alpha + p\zeta/q + \tilde{\theta}(\zeta)$ , where  $\alpha$  is a fieldline label;  $p$  and  $q$  are integers that determine periodicity; and  $\tilde{\theta}(0) = \tilde{\theta}(2\pi q) = 0$ .
4. On *each* curve,  $\rho_\alpha(\zeta) = P(\theta_\alpha(\zeta), \zeta)$  and  $\theta_\alpha(\zeta)$ , can enforce  $\frac{\partial S}{\partial\rho} = 0$ ; generally  $\nu \equiv \frac{\partial S}{\partial\theta} \neq 0$ .
5. The *pseudo* surface dynamics is defined by  $\dot{\theta} \equiv B^\theta/B^\zeta$  and  $\dot{\rho} \equiv \partial_\theta P \dot{\theta} + \partial_\zeta P$ .
6. Corresponding *pseudo* field  $\mathbf{B}_\nu \equiv \dot{\rho} B^\zeta \mathbf{e}_\rho + \dot{\theta} B^\zeta \mathbf{e}_\theta + B^\zeta \mathbf{e}_\zeta$ ; simplifies to  $\mathbf{B}_\nu = \mathbf{B} - \frac{\nu}{\sqrt{g}} \mathbf{e}_\rho$ .
7. Introduce the quadratic-flux functional:  $\boxed{\varphi_2 \equiv \frac{1}{2} \iint d\theta d\zeta \left( \frac{\partial S}{\partial\theta} \right)^2}$
8. Allowing for  $\delta P$ , the first variation is  $\delta\varphi_2 = \iint d\theta d\zeta \delta P \sqrt{g} \underbrace{(B^\theta \partial_\theta + B^\zeta \partial_\zeta)}_{\text{Euler-Lagrange for QFMs}} \nu$ .

# Alternative Lagrangian integration construction: QFM surfaces are families of extremal curves of the constrained-area action integral.

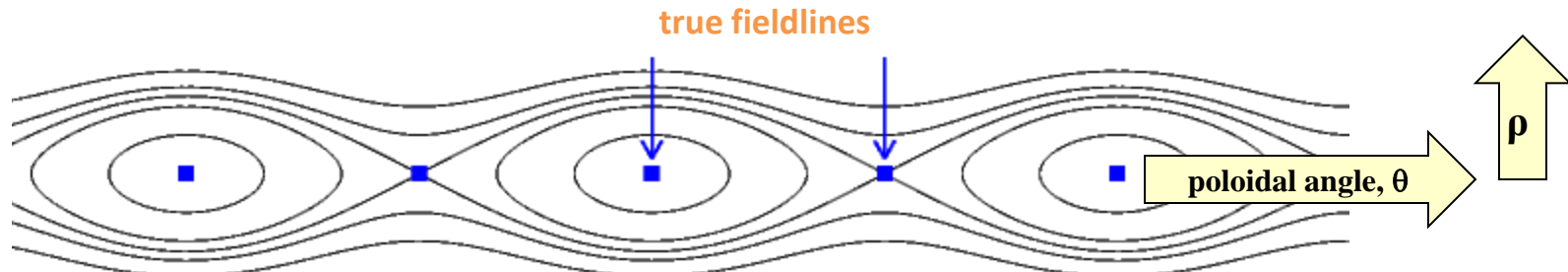
1. Introduce  $F(\boldsymbol{\rho}, \boldsymbol{\theta}) \equiv \int_{\mathcal{C}} \mathbf{A} \cdot d\mathbf{l} - \nu \left( \int_{\mathcal{C}} \theta \nabla \zeta \cdot d\mathbf{l} - a \right)$ , where  $\boldsymbol{\rho} \equiv \{\rho_i\}$ ,  $\boldsymbol{\theta} \equiv \{\theta_i\}$ ;  
where  $\nu$  is a Lagrange multiplier, and  $a$  is the required “area”,  $\int_0^{2\pi q} \theta(\zeta) d\zeta$ .
2. An identity of vector calculus gives  $\delta F = \int_{\mathcal{C}} d\mathbf{l} \times (\nabla \times \mathbf{A} - \nu \nabla \theta \times \nabla \zeta) \cdot \delta \mathbf{l}$ ,  
extremizing curves are tangential to  $\mathbf{B} - \nu \nabla \theta \times \nabla \zeta = \mathbf{B} - \frac{\nu}{\sqrt{g}} \mathbf{e}_{\rho} = \mathbf{B}_{\nu}$ .
3. Constrained-area action-extremizing curves satisfy  $\frac{\partial F}{\partial \rho_i} = 0$  and  $\frac{\partial F}{\partial \theta_i} = 0$ .
4. The piecewise-constant representation for  $\rho(\zeta)$  and  $\partial_{\rho_i} F = 0$  yields  $\rho_i = \rho_i(\theta_{i-1}, \theta_i)$ , so  
the trial curve is completely described by  $\theta_i$ , i.e.  $F \equiv F(\boldsymbol{\theta})$ .
5. The piecewise-linear representation for  $\theta(\zeta)$  gives  $\frac{\partial F}{\partial \theta_i} = \partial_2 F_i(\theta_{i-1}, \theta_i) + \partial_1 F_{i+1}(\theta_i, \theta_{i+1})$ ,  
so the Hessian,  $\nabla^2 F(\boldsymbol{\theta})$ , is tridiagonal (assuming  $\nu$  is given) and is easily inverted.
6. Multi-dimensional Newton method:  $\delta \boldsymbol{\theta} = -(\nabla^2 F)^{-1} \cdot \nabla F(\boldsymbol{\theta})$ ;  
*global* integration, much less sensitive to “Lyapunov” integration errors.

The action gradient,  $\nu$ , is constant along the pseudo fieldlines; construct Quadratic Flux Minimizing (QFM) surfaces by pseudo fieldline (local) integration.

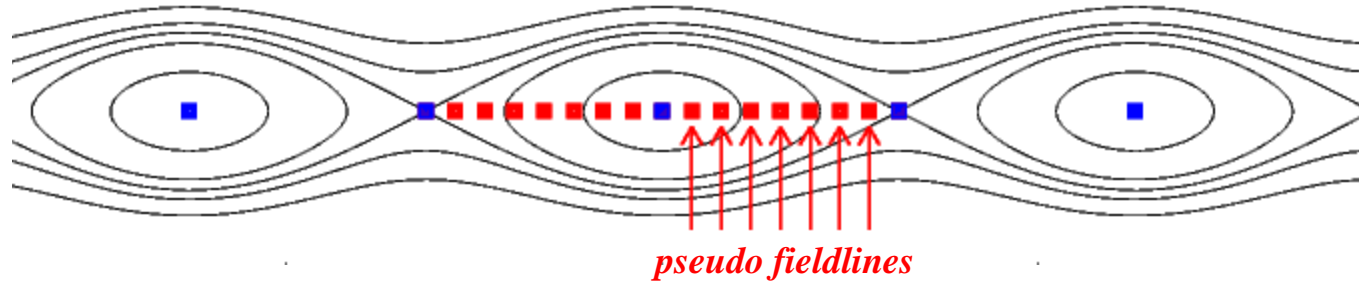
1. The *true* fieldline flow along  $\mathbf{B}$  around  $q$  toroidal periods from  $(\theta_0, \rho_0)$  produces a mapping,  $\begin{pmatrix} \theta_q \\ \rho_q \end{pmatrix} = M^q \begin{pmatrix} \theta_0 \\ \rho_0 \end{pmatrix}$ .
2. Periodic fieldlines are fixed points of  $M^q$ , i.e.  $\theta_q = \theta_0 + 2\pi p$ ,  $\rho_q = \rho_0$ .
3. In integrable case: given  $\theta_0$ , a one-dimensional search in  $\rho$  is required to find the *true* periodic fieldline.
4. In non-integrable case, only the
  - (i) “stable” (action-minimax),  $O$ , (which is not always stable), and the
  - (ii) unstable (action minimizing),  $X$ , periodic fieldlines are guaranteed to survive.
5. The *pseudo* fieldline flow along  $\mathbf{B}_\nu = \mathbf{B} - \frac{\nu}{\sqrt{g}} \mathbf{e}_\rho$  around  $q$  periods from  $(\theta_0, \rho_0)$  produces a mapping,  $\begin{pmatrix} \theta_q \\ \rho_q \end{pmatrix} = P^q \begin{pmatrix} \nu \\ \rho_0 \end{pmatrix}$ , but  $\nu$  is not yet known.
6. In general case: given  $\theta_0$ , a two-dimensional search in  $(\nu, \rho)$  is required to find the periodic *pseudo* fieldline.

# Lagrangian integration is sometimes preferable, but not essential: can iteratively compute radial “error” field

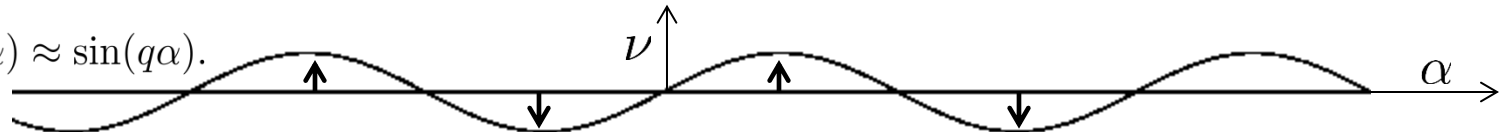
0. Usually, there are only the “stable” periodic fieldline and the unstable periodic fieldline,



1. At every  $\theta = \alpha$ , determine  $\nu(\alpha)$  via numerical search so that  $\mathbf{B} - \nu \mathbf{e}_\rho / \sqrt{g}$  yields a periodic integral curve; where  $\alpha$  is a fieldline label.



2. At the true periodic fieldlines, the required additional radial field is zero: i.e.  $\nu(\alpha_0) = 0$  and  $\nu(\alpha_X) = 0$ .
3. Typically,  $\nu(\alpha) \approx \sin(q\alpha)$ .



4. The pseudo fieldlines “capture” the true fieldlines; QFM surfaces pass through the islands.

A magnetic vector potential, in a suitable gauge,  
is quickly determined by radial integration.

1. Generally, gauge freedom allows  $\mathbf{A} = A_\theta(\rho, \theta, \zeta) \nabla \theta + A_\zeta(\rho, \theta, \zeta) \nabla \zeta$ .

2.  $\nabla \times \mathbf{B} = \mathbf{A}$  gives

$$\begin{aligned}\sqrt{g}B^\rho &= \partial_\theta A_\zeta - \partial_\zeta A_\theta, \\ \sqrt{g}B^\theta &= \quad \quad \quad - \partial_\rho A_\zeta, \\ \sqrt{g}B^\zeta &= \partial_\rho A_\theta.\end{aligned}$$

3. Given the magnetic field,  $\mathbf{A}$  is quickly determined by radial integration in Fourier space:

$$\begin{aligned}\partial_\rho A_{\theta,m,n} &= +(\sqrt{g}B^\zeta)_{m,n}, \\ \partial_\rho A_{\zeta,m,n} &= -(\sqrt{g}B^\theta)_{m,n},\end{aligned}$$

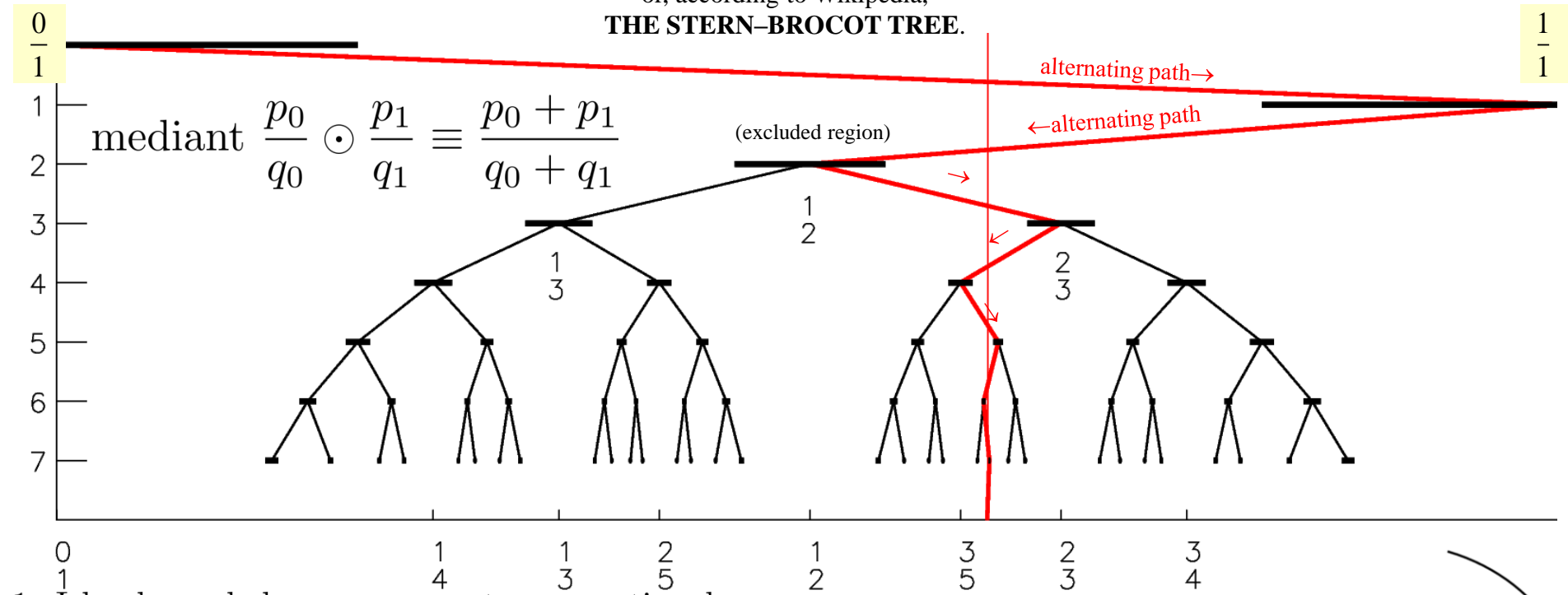
and the 3<sup>rd</sup> equation,  $\sqrt{g}B^\rho = \partial_\theta A_\zeta - \partial_\zeta A_\theta$ , is satisfied if  $\nabla \cdot \mathbf{B} = 0$ ;  
present implementation assumes coordinate axis coincides with magnetic axis,  
which causes a problem for sawteeth . .

4. Hereafter, use notation  $\mathbf{A} = \psi \nabla \theta - \chi \nabla \zeta$ .

# The structure of phase space is related to the structure of rationals and irrationals.

## THE FAREY TREE;

or, according to Wikipedia,  
THE STERN–BROCOT TREE.



1. Islands, and chaos, emerge at every rational:

about each rational,  $n/m$ , introduce “excluded region” with width  $r/m^k$ ; if excluded regions don’t overlap, then

2. KAM theorem: irrational flux surface can survive if  $|t - n/m| > r/m^k$  for all  $n, m$ .

Call  $t$  *strongly irrational*.

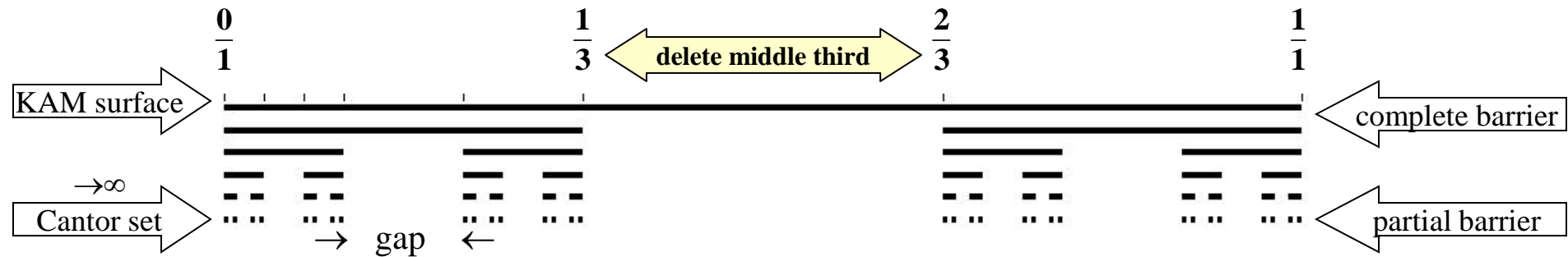
Diophantine condition

3. Greene’s residue criterion: the most robust flux surfaces have “noble” transform:

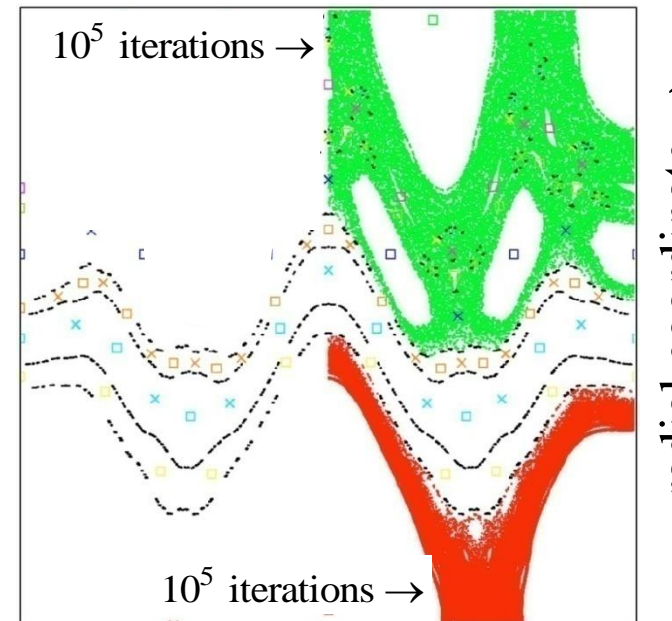
noble irrationals  $\equiv$  limit of ultimately alternating paths  $\equiv$  limit of Fibonacci ratios;

e.g.  $\frac{0}{1}, \frac{1}{0}, \frac{1}{1}, \frac{2}{1}, \frac{3}{2}, \frac{5}{3}, \frac{8}{5}, \frac{13}{8}, \frac{21}{13}, \frac{34}{21}, \frac{55}{34}, \dots \rightarrow \gamma \equiv$  golden mean  $\equiv \frac{(1+\sqrt{5})}{2}$ ; e.g.  $\frac{1}{0}, \frac{0}{1}, \frac{1}{1}, \frac{1}{2}, \frac{2}{3}, \frac{3}{5}, \frac{5}{8}, \frac{8}{13}, \frac{13}{21}, \frac{21}{34}, \dots \rightarrow \gamma^{-1}$ .

Irrational KAM surfaces break into cantori when perturbation exceeds critical value.  
 Both KAM surfaces and cantori restrict transport.



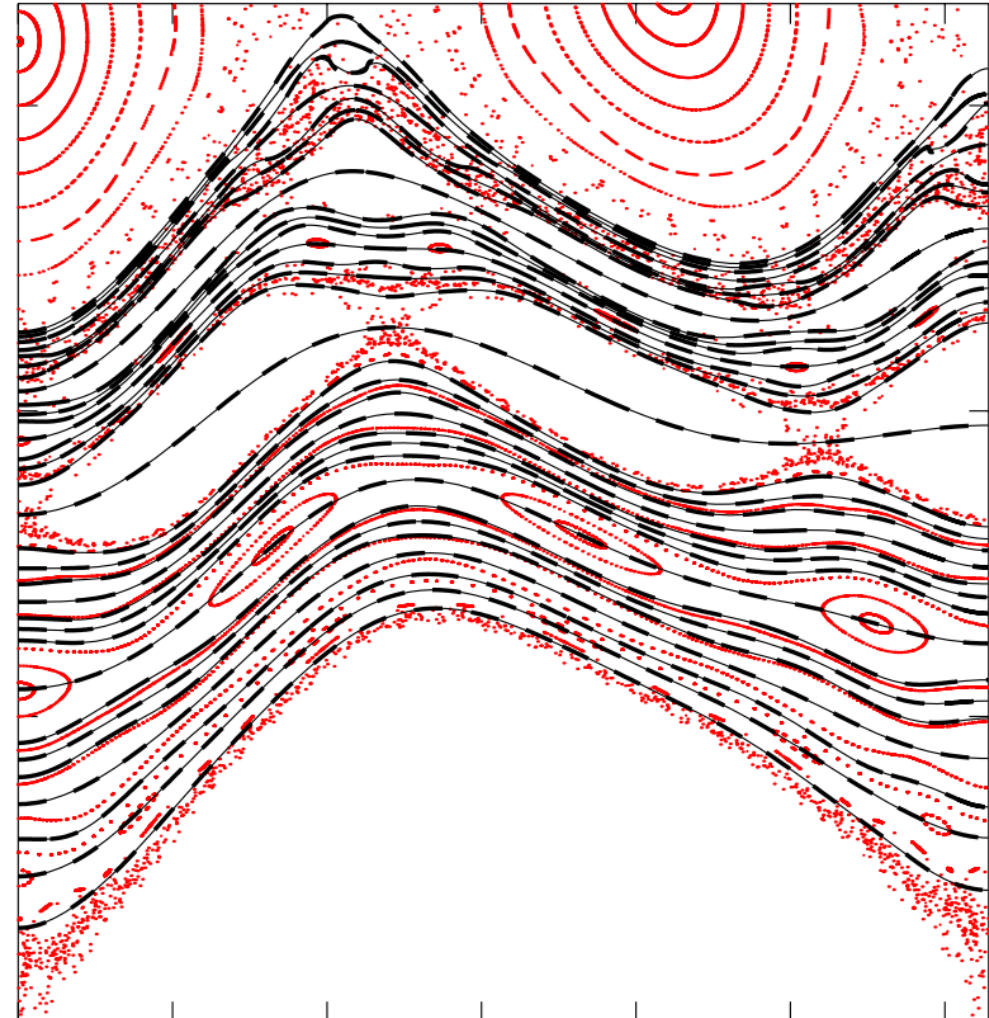
- KAM surfaces are closed, toroidal surfaces that **stop** radial field line transport
- Cantori have “gaps” that fieldlines can pass through; however, **cantori can severely restrict** radial transport
- Example: all flux surfaces destroyed by chaos, “**noble**” cantori (black dots) but even after **100 000 transits** around torus the fieldlines **don’t get past cantori** !
- Regions of chaotic fields can provide some confinement because of the cantori partial barriers.



# Ghost surfaces are (almost) indistinguishable from QFM surfaces

can redefine poloidal angle to unify ghost surfaces with QFMs.

1. Ghost-surfaces are defined by an (action gradient) flow.
2. QFM surfaces are defined by minimizing  $\int (\text{action gradient})^2 ds$ .
3. Not obvious if the different definitions give the same surfaces.
4. For model chaotic field:
  - (a) ghosts = thin solid lines;
  - (b) QFMs = thick dashed lines;
  - (c) agreement is excellent;
  - (d) difference =  $\mathcal{O}(\epsilon^2)$ , where  $\epsilon$  is perturbation.
5. Can redefine  $\theta$  to obtain unified theory of ghosts & QFMs; straight *pseudo* fieldline angle.



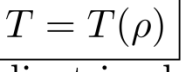
# Isotherms of the steady state solution to the anisotropic diffusion coincide with ghost surfaces; analytic, 1-D solution is possible.

1. Transport along the magnetic field is unrestricted:  
e.g. parallel random walk with long steps  $\approx$  collisional mean free path.
2. Transport across the magnetic field is very small:  
e.g. perpendicular random walk with short steps  $\approx$  Larmor radius.

3. Simple transport model: anisotropic diffusion,

$$\kappa_{\parallel} \nabla_{\parallel}^2 T + \kappa_{\perp} \nabla_{\perp}^2 T = 0, \quad \kappa_{\perp}/\kappa_{\parallel} \sim 10^{-10}, \text{ grid } = 2^{12} \times 2^{12}.$$

steady state, no source, inhomogeneous boundary conditions.

4. Compare numerical solution to “irrational” ghost-surfaces 
5. The temperature adapts to KAM surfaces, cantori, and ghost-surfaces!, i.e.  $T = T(\rho)$ .
6. From  $T = T(\rho, \theta, \zeta)$  to  allows an expression for the temperature gradient in chaotic fields:

$$\frac{dT}{d\rho} \propto \frac{1}{\kappa_{\parallel} \varphi_2 + \kappa_{\perp} G},$$

where  $\varphi_2 \equiv \underbrace{\int B_n^2 ds}_{\text{quadratic flux}}$ , and  $G \equiv \underbrace{\int \nabla \rho \cdot \nabla \rho ds}_{\text{metric}}$ .

